Macromolecules

pubs.acs.org/Macromolecules Article

Intermicellar Polymerization and Intramicellar Cyclization: A Supramolecular Ring−Chain Competition Reaction

Rui Hu, Liang Gao,* Chunhua Cai, Jiaping Lin,* Zuowei Chen, and Liquan Wang

Cite This: *Macromolecules* 2021, 54, 5196−5203 Read Online

ACCESS | Metrics & More | Article Recommendations | Supporting Information

ABSTRACT: At the molecular level, intermolecular polymerization can compete with its intramolecular cyclization, which is known as a ring−chain competition reaction. However, this competitive phenomenon has rarely been observed in higher-level systems. Herein, we report a supramolecular ring−chain competition reaction between the intermicellar polymerization and intramicellar cyclization of rodlike micelles assembled from rod−coil graft copolymers. Nanowires and toroidal micelles are the chain-like and ring-like products of the two supramolecular reactions, respectively. When the reaction conditions (solvent composition or temperature) are varied, the competition of the two supramolecular reactions is induced, and their dynamic competition relation and equilibrium constants can be regulated by the reaction conditions. The combination of experiments and theoretical simulations reveals that the interplay of the core/shell interfacial energy, the bending energy of rodlike micelles, and the end-capping energy determines such ring−chain competition. This study presents an advance in supramolecular self-assembly and provides a progressive way to construct complex hierarchical nanostructures.

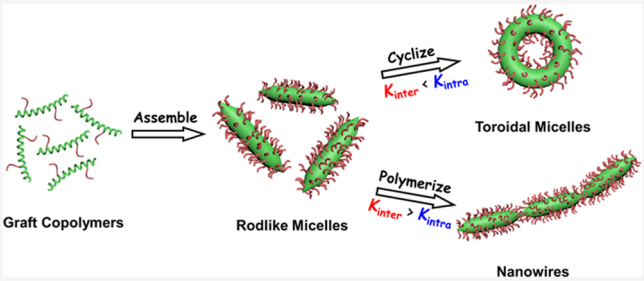

INTRODUCTION

Ring−chain equilibrium between intermolecular coupling and intramolecular cyclization, which is a common competitive reaction at the molecular level, affects the molecular structures and yields of products.[1−6] For instance, in the enzyme-catalyzed synthesis process of aliphatic and unsaturated polyesters, cyclic oligomers are formed concurrently with the corresponding linear chains, and the yield of cyclic oligomers depends on the monomer structure and the initial monomer concentration.[3,7,8] Even for the oligomer reaction units, the macrocyclization reaction can compete with their polymerization driven by the fast association and dissociation of reversible noncovalent interactions.[9−11] For such a system, it was found that the concentration of cyclic counterparts is influenced by the concentration and linker length of oligomer building blocks.[9−11] Thus, competition is crucial when attempting to obtain a high yield of linear or ring-like products or to build an exquisite buffering system.[1,12] However, the competitive reaction has rarely been observed in higher-level systems (higher level refers to the assembly of polymeric micellar subunits, which occurs at the nanoscale).[13−19]

Complex hierarchical nanostructures can be constructed through the higher-level assembly of the preassembled micelle subunits.[20−25] For example, Lin et al. reported that poly(γ-benzyl-L-glutamate)-*g*-poly(ethylene glycol) (PBLG-*g*-PEG) can self-assemble into rodlike micelles, and the preassembled micelles can further assemble into nanowires.[26−28] In the rodlike micelles of rod−coil graft copolymers, rigid backbones take a parallel packing manner in the micellar core, and the imperfect coverage of the micellar core by the coil grafts leads to high-energy micellar ends. The rodlike micelles assemble into nanowires to eliminate the high-energy micellar ends, resembling a polymerization reaction (referred to as supramolecular polymerization), but the monomers are polymeric micelles.

In addition to forming nanowires, such polypeptide rodlike micelles can cyclize into toroids in an end-to-end closure manner under certain conditions.[29,30] This self-assembly behavior is attributed to the interplay of the core/shell interfacial energy, the bending energy of rodlike micelles, and the end-capping energy. The cyclization phenomenon of rodlike micelles resembles the intramolecular cyclization of monomers or oligomers, but it occurs at a supramolecular level and is referred to as supramolecular cyclization. However, is there a ring−chain competition reaction at this supramolecular level? Moreover, revealing the competitive mechanism between two supramolecular reactions (polymerization and

Received: May 10, 2021
Published: May 24, 2021

https://doi.org/10.1021/acs.macromol.1c01020
Macromolecules 2021, 54, 5196−5203

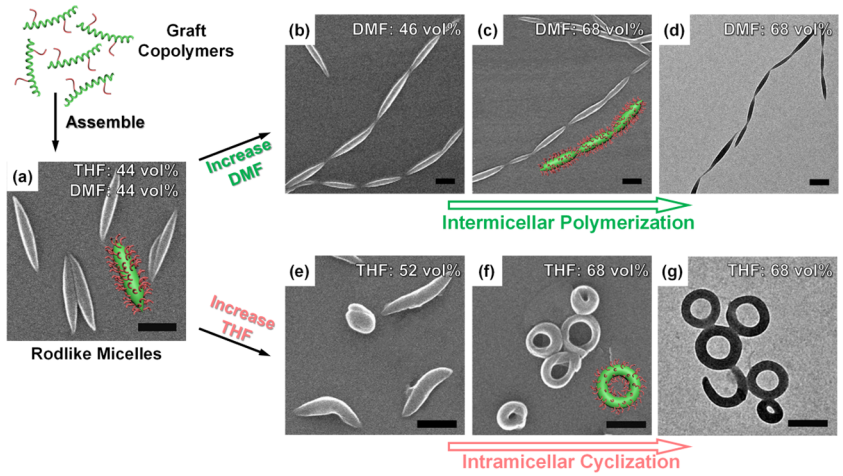

Figure 1. SEM images of (a) the rodlike micelles of $PBLG_{822}$-*g*-PEG_{17} and (b, c, e, f) the aggregates generated from the rodlike micelles with increasing DMF or THF content. (d, g) The corresponding TEM images of (c) and (f), respectively. The preparation temperature in (a–g) is fixed at 30 °C. Scale bar: 300 nm.

cyclization) and realizing precise controls of nanostructures is a significant advance in supramolecular self-assembly.

Herein, we report unique supramolecular ring–chain competition between the intermicellar polymerization and the intramicellar cyclization of rodlike micelles assembled from PBLG-*g*-PEG graft copolymers. The supramolecular competition can be regulated by varying the solvent composition and temperature. Energy variations calculated from theoretical simulations reveal the origin of such supramolecular ring–chain competition. The equilibrium constants of the intermicellar and intramicellar reactions are evaluated to reveal their dynamic competition. This study provides a promising way to construct controllable nanoassemblies.

RESULTS AND DISCUSSION

Intermicellar Polymerization and Intramicellar Cyclization of Rodlike Micelles. Rodlike micelles were assembled from $PBLG_{822}$-*g*-PEG_{17} graft copolymers (the subscript represents the number of repeating units for each segment, and the details of polymer synthesis are given in Section 1.1 of the Supporting Information). In the experiments, 0.56 mL of water (a selective solvent for PEG) was added into 4.0 mL of the tetrahydrofuran/dimethylformamide (THF/DMF) solution of copolymers (THF:/DMF, 5:5 by volume, the polymer concentration is 0.3 g/L) to prepare the rodlike micelles. Figure 1a shows the scanning electron microscopy (SEM) image of the morphologies of the $PBLG_{822}$-*g*-PEG_{17} rodlike micelles. The mean length and the aspect ratio of the rodlike micelles are 600 ± 28 nm and 6.13 ± 0.31, respectively, as estimated from the SEM images of more than 400 micelles. Note that the samples for SEM measurements were prepared from the micellar aqueous solution obtained by dialyzing against deionized water (see Section 1.2 of the Supporting Information). During the dialyzing process, the aggregate morphologies are frozen, which can rule out the effect of THF or DMF evaporation.

Then, 1.6 mL of the mixed solvent with various THF/DMF contents and 0.4 mL of water were added into 1.0 mL of the micelle solution (THF/DMF/water, 44:44:12 by volume). The final contents of DMF and THF can be regulated by varying the THF/DMF ratio of the added mixed solvent. As the DMF content or THF content increases, two different supramolecular self-assemblies occur. At higher DMF content, nanowires are formed via the end-to-end connection of rodlike micelles (i.e., supramolecular polymerization, Figures 1b–d and S3). The dynamic light scattering (DLS) results show that the apparent hydrodynamic radius (R_h) values gradually increase, and its distribution becomes broader with increasing DMF content (Figure S4), indicating that nanowires are formed in the solution. We carried out cryogenic transmission electron microscopy (Cryo-TEM) measurements on the solution of rodlike micelles and nanowires. The nodes between the neighboring rodlike micelles in Cryo-TEM images (see Figure S5) suggest that the intermicellar polymerization occurs in the solution.

In the rodlike micelles, the PBLG backbones take a parallel packing within the micellar core, and the PEG grafts form the corona to stabilize the micelles. At the micellar ends, the PBLG cores cannot be entirely covered by PEG, resulting in the partially exposed ends with higher energy. The increase in DMF content can lead to the swelling of the PBLG cores, resulting in more exposure of the active ends. Thus, the nanowires are formed. The supramolecular polymerization mechanism is further confirmed by two control experiments (Figure S6), which verifies the fact that the nanowires are formed through the elimination of the high-energy ends.

As the THF content increases, the supramolecular cyclization reaction occurs. Figure 1e–g show the curved and toroidal micelles generated from the rodlike micelles at higher THF contents. The average diameter of the toroids is 197 ± 19 nm, and the circumference is 618 ± 60 nm, which is close to the mean length (600 nm) of the initial rodlike micelles. This indicates that the toroids are formed via the end-to-end closure of the rodlike micelles (i.e., supramolecular cyclization). The R_h values remain unchanged with increasing THF content, suggesting that the cyclization of rodlike micelles in the solution is an intramicellar reaction (Figure S4). The Cryo-TEM image of the toroids (Figure S5) further confirms that intramicellar cyclization occurs in the solution. The supramolecular cyclization phenomenon is related to the interplay of the core/shell interfacial energy, the bending energy of rodlike micelles, and the end-capping energy.[29,30]

Under certain conditions, the unclosed curved micelles tend to connect with each other during the cyclization process due

https://doi.org/10.1021/acs.macromol.1c01020
Macromolecules 2021, 54, 5196–5203

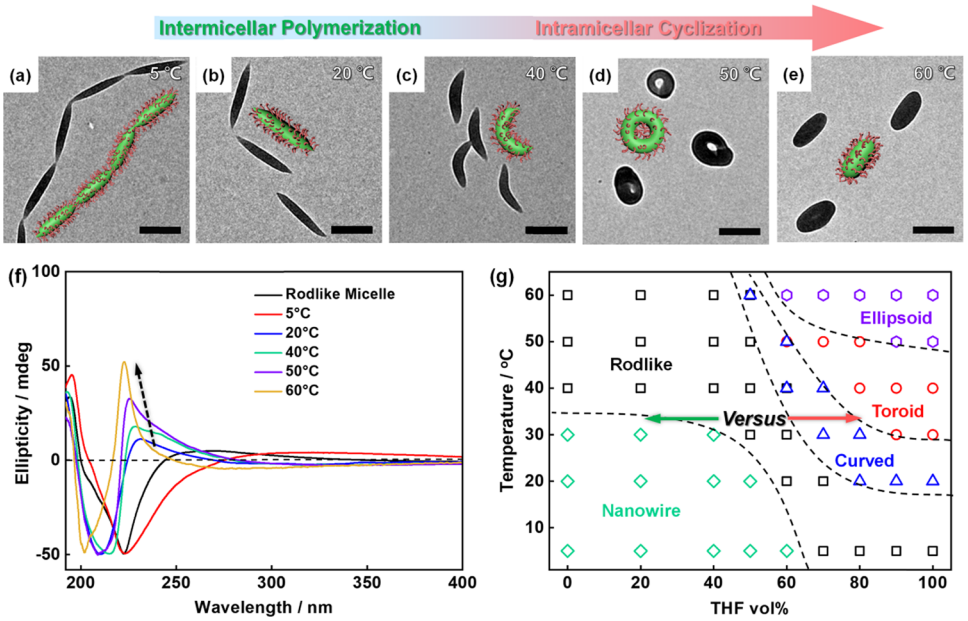

Figure 2. (a–e) TEM images of the aggregates generated from rodlike micelles after adding the THF/DMF mixture solvent (6/4, v/v) at various temperatures, where the final THF content is fixed at 46 vol %. Scale bar: 300 nm. (f) Circular dichroism (CD) spectra of the initial rodlike micelles and the formed aggregates at various temperatures and the fixed THF content of 46 vol %. The arrow guides the variation of the bands related to the pendant groups. (g) Morphological diagram of the aggregates generated from rodlike micelles in the space of temperature and the THF content in the added mixed solvent.

to the competition between polymerization and cyclization (Figure S7). Additionally, we examined the effect of copolymer structures. For example, with respect to the rodlike micelles formed by $PBLG_{548}$-*g*-PEG_{17} with a shorter PBLG backbone, its aspect ratio decreases to 3.8 ± 0.3. The shorter rodlike micelles can assemble into nanowires at higher DMF content or bend into curved micelles at higher THF content (Figure S8). Therefore, by varying the solvent composition, ring–chain competition occurs in this higher-level self-assembly system. We termed the competition between the intermicellar polymerization and the intramicellar cyclization as a supramolecular ring–chain competition reaction.

Supramolecular Ring–Chain Competition Reaction of Rodlike Micelles. To gain insights into such supramolecular competition, the effect of temperature was examined in addition to the solvent composition. The mixed solvent (1.6 mL, THF/DMF, 6:4 by volume) and water (0.4 mL) were added into 1.0 mL of the rodlike micelle solution, and then the mixture micelle solution was stabilized for 3 days at various temperatures. The morphologies of the formed aggregates were characterized by SEM, transmission electron microscopy (TEM), and atomic force microscopy (AFM). As shown in Figures 2a–d and S9, with increasing temperature from 5 to 50 °C, nanowires, rodlike, curved, and toroidal micelles can be observed. This means that the supramolecular polymerization occurs at lower temperatures, while its cyclization reaction becomes dominant at higher temperatures. With further increasing the temperature to 60 °C, the toroidal micelles collapse into ellipsoidal aggregates (Figure 2e).

To reveal the supramolecular competition mechanism, we performed the turbidity (optical density, OD) measurements of $PBLG_{822}$ homopolymers at various temperatures, and then carried out circular dichroism (CD) experiments on the solutions of $PBLG_{822}$-*g*-PEG_{17} micelles formed at various temperatures. According to the OD results (Figure S10), the critical water content of $PBLG_{822}$ for aggregation decreases from 7.9 vol % at 50 °C to 6.3 vol % at 5 °C, which indicates that the hydrophobicity of PBLG increases as the temperature decreases.[28] At lower temperatures, the partial exposure of the micellar core with stronger hydrophobic PBLG leads to higher end-capping energy at the micellar ends. Thus, eliminating the unfavorable micellar ends leads to the polymerization of rodlike micelles.

CD measurements can provide the conformation information of PBLG segments and the packing manners of their pendant phenyl groups. As shown in Figure 2f, all of the CD spectra present a positive peak (230–280 nm) and a negative peak (200–230 nm). The signal at 200–230 nm is attributed to the right-handed α-helix conformation of PBLG segments. The region at 230–280 nm represents the chiral arrangement of the pendant phenyl groups on the PBLG backbones.[31−36] The positive band at 230–280 nm indicates a shrunken left-handed arrangement, and the negative signal corresponds to a loosely packed right-handed arrangement.[31−36] With increasing temperature, the intensity of the positive signals of pendant phenyl groups around 230 nm gradually increases (see the arrow in Figure 2f), and the peaks shift toward the shorter wavelengths. This indicates that higher temperatures enhance the left-handed arrangement of pendant groups, that is, the packing manner of pendant groups becomes more ordered. This constriction leads to higher unfavorable core/shell interfacial energy.[29] To offset this energy variation, the rodlike micelles bend into curved micelles and then cyclize into toroidal micelles to reduce the interfacial energy (the interfacial area is decreased). It is also observed from CD that an increase in THF content can give rise to a constriction of the pendant groups (Figure S11). This constriction results in higher unfavorable core/shell interfacial energy, inducing the intramicellar cyclization at the higher THF content. Therefore, the stronger hydrophobicity of PBLG at lower

https://doi.org/10.1021/acs.macromol.1c01020
Macromolecules 2021, 54, 5196−5203

temperatures is responsible for the intermicellar polymerization, while the increasing core/shell interfacial energy at higher temperatures or higher THF contents gives rise to the intramicellar cyclization.

Summarizing the experimental data, we constructed a morphological diagram of the generated aggregates to show the supramolecular ring−chain competition under various conditions. Here, the THF content in the added mixed THF/DMF solvent varies from 0 to 100 vol %, and the temperature varies from 5 to 60 °C. We mapped out the morphological diagram with THF content versus temperature. As shown in Figure 2g, the morphological diagram consists of five zones, including rodlike, nanowire, curved, toroidal, and ellipsoidal micelles. The nanowires are formed at lower temperatures and lower THF content, where eliminating the high-energy micellar ends is the main driving force for supramolecular polymerization. The initial rodlike micelles remain unchanged in the medium region of the diagram. With increasing temperature or THF content, the rodlike micelles gradually bend into curved micelles. The toroidal micelles are obtained when the temperature is above 30 °C, and the THF content in the added mixed solvent is above 80 vol %. In this region, the variation of the core/shell interfacial energy plays a dominant role in supramolecular cyclization. Further increasing the temperature is unfavorable to the stability of toroids, and toroids collapse into ellipsoid micelles. Higher temperatures lead to the stronger constriction of PBLG pendant groups, generating higher core/shell interfacial energy. As a result, the rigidity of micelles cannot maintain the toroids, and the collapsed ellipsoids are formed.

To support the proposed mechanism, we carried out a control experiment. The micelles solution was dialyzed to be an aqueous solution, and the intermicellar polymerization of rodlike micelles cannot be observed, while their cyclization still occurs (Figure S12). It is believed that the dialysis shrinks the hydrophobic PBLG core, reduces the exposed area at the micellar ends, and results in the elimination of reactive points. Thus, the high-energy end is crucial for supramolecular polymerization but plays a less important role in the cyclization process.

Theoretical Simulations of the Supramolecular Competition Reaction. To further reveal the mechanism of the supramolecular competition reaction, we performed Brownian dynamic (BD) simulations on the supramolecular reaction of the rodlike micelles. First, a coarse-grained BD model of the R_m-g-$(C_n)_2$ graft copolymer was constructed (Figure 3a). R_m-g-$(C_n)_2$ contains one backbone and two grafted side chains, where R and C beads represent the PBLG backbone and the PEG graft, respectively. One P bead is connected to each R bead to represent the pendant groups of the PBLG backbones. The subscripts denote the bead numbers, and they are chosen as m = 16 and n = 4 to match the relative lengths of PBLG and PEG segments for the $PBLG_{822}$-g-PEG_{17} copolymer used in the experiments. Thus, the graft copolymer is modeled as R_{16}-g-$(C_4)_2$. The angle bending potential describes the rigidity of the PBLG backbone. All of the pairwise interactions are described by the standard Lennard-Jones (LJ) potentials with different cutoff radii.[37−39] The hydrophobicity of PBLG is simulated by an attractive LJ potential for R−R pairwise interaction, and its strength is denoted by the interaction parameter ε_{RR}. The hydrophilicity of PEG and the incompatibility between PEG and PBLG segments are described by setting the repulsive potentials for

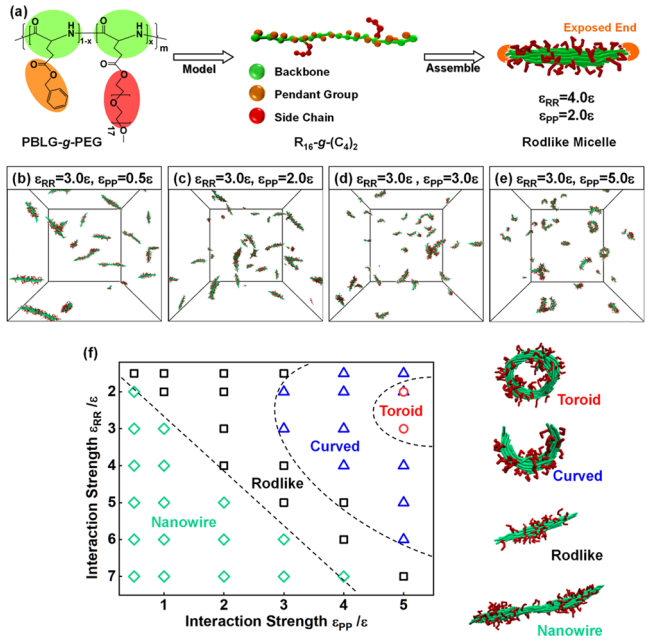

Figure 3. (a) BD model of a rod-g-coil graft copolymer and the representative simulation structure of rodlike micelle. (b−e) Simulation snapshots of aggregates generated from the initial rodlike micelles under different groups of interaction parameters. (f) Morphological diagram of simulation aggregates generated from rodlike micelles in the space of ε_{RR} and ε_{PP}. The right side shows the representative simulation structures.

C−C and R−C pairwise interactions, respectively. To describe the noncovalent interaction between the pendant phenyl groups, the P−P interaction is modeled as an attractive LJ potential, and the P−P interaction strength is denoted by ε_{PP}.[29,30] The setting and variation of simulation parameters match the assembly conditions in the experiments. The other parameter settings in the simulations are shown in Section 2 of the Supporting Information.

As shown in Figure 3a, the rodlike micelles are formed by R_{16}-g-$(C_4)_2$ under the condition of ε_{RR} = 4.0ε and ε_{PP} = 2.0ε (Figure S14). The simulation morphology of rodlike micelles shows that the rigid backbones in the micellar core take an ordered parallel packing manner and the coil side chains in the corona stabilize the rodlike micelles. At the micellar ends, the imperfect coverage of coil side chains onto the micellar core is observed (see the marked regions in Figure 3a). These partially exposed ends can serve as reaction points in the supramolecular reactions. We took out the preassembled rodlike micelles and randomly dispersed them into another simulation box. Then, ε_{RR} and ε_{PP} were varied to simulate the variations of solvent composition and temperature. Higher ε_{RR} corresponds to the stronger hydrophobicity of the PBLG backbones with decreasing temperature in the experiments. The increase of ε_{PP} corresponds to the constriction of the pendant phenyl groups of PBLG with increasing temperature or THF content (i.e., the increase of the core/shell interfacial energy) (see Figure 2f). Figure 3b−e shows the representative simulation morphologies obtained under four groups of simulation conditions. When ε_{RR} is fixed at 3.0ε, with increasing ε_{PP} from 0.5ε to 5.0ε, nanowires, rodlike, curved, and toroidal micelles are obtained. This indicates that the supramolecular polymerization of rodlike micelles occurs at lower ε_{PP}, while its cyclization reaction is dominant at higher ε_{PP}. The simulation results well

https://doi.org/10.1021/acs.macromol.1c01020
Macromolecules 2021, 54, 5196−5203

reproduce the two supramolecular reactions of rodlike micelles.

To reveal the competitive relation between two kinds of interactions, the effects of the interaction parameters ε_{RR} and ε_{PP} on such a ring−chain competition reaction were examined systematically. According to the simulation results, a morphological diagram of the generated aggregates in the simulations was constructed. Four regions, including nanowires, rodlike, curved, and toroidal micelles, are shown in the phase diagram (Figure 3f). Nanowires are formed in the region of high ε_{RR} and low ε_{PP}, and the supramolecular cyclization occurs in the region of low ε_{RR} and high ε_{PP}. It is noted that appropriately adjusting the simulation parameters could give rise to an overlapping phase boundary. Coexistence regions containing two structures (e.g., curved micelles and connected curved micelles) appear. Such a variation suggests that the composition of final products can be tuned by the reaction conditions.

Mechanism and the Theoretical Model of the Supramolecular Ring−Chain Competition Reaction. The energy variations during the ring−chain competition process were calculated to reveal the origin of such competition. The total energy E of rodlike micelles contains the core/shell interfacial energy E_{inter}, the bending energy E_{bend}, and the end-capping energy E_{end}.[40,41] E_{bend} can be evaluated from the angle potential of the copolymer backbones, and E_{end} and E_{inter} can be obtained from the pairwise LJ potential of all the coarse-grained beads at the exposed micellar ends and on the micellar interface, respectively.[29] The energy variations were calculated from the initial rodlike micelles to the generated aggregates under different conditions (for details, see Section 2.3 of the Supporting Information).

According to the morphological diagram (Figure 3f), we chose the simulation condition of $\varepsilon_{RR} = 3.0\varepsilon$ and varied the ε_{PP} to induce the polymerization or cyclization of the rodlike micelles, corresponding to varying temperatures at the fixed THF content in the experiments. The energy variations during the competition process are presented in Figure 4. In the left region of Figure 4, with decreasing ε_{PP}, E_{end} and E_{inter} gradually decrease, while E_{bend} shows only a slight decrease. The total energy E goes down significantly and the nanowires are formed. As can be seen, the variation of E_{end} contributes mainly to the decrease of E. This result indicates that the intermicellar polymerization is mainly related to the elimination of exposed micellar ends with high end-capping energy (E_{end}). In contrast, with increasing ε_{PP}, cyclization of rodlike micelles occurs, and the total energy E gradually decreases (see Figure 4). During this intramicellar cyclization process, E_{inter} shows a significant decrease, E_{bend} rapidly increases, and E_{end} decreases when toroids are eventually formed. The results indicate that the two supramolecular reactions present different evolution pathways. When the energy variations of E_{inter} and E_{bend} dominate, cyclization occurs. Conversely, the rodlike micelles polymerize into nanowires when the variation of E_{end} serves as the main energy contribution. The supramolecular ring−chain competition reaction is a result of the interplay of the interfacial energy, the bending energy, and the end-capping energy of micelles.

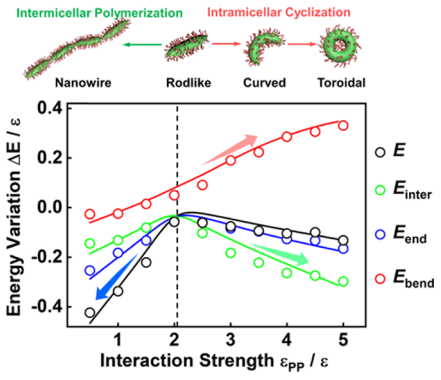

Figure 4. Variations of the bending energy E_{bend}, the end-capping energy E_{end}, the interfacial energy E_{inter}, and the total energy E in the supramolecular ring−chain competition. The energy variations were calculated from the pairwise interaction potential and the angle potential in the simulations, where ε_{PP} varies from 0.5ε to 5.0ε at a fixed ε_{RR} of 3.0ε.

In addition, we examined the dynamic competition process and proposed a ring−chain equilibrium model. The Jacobson−Stockmayer (JS) theoretical model well describes the ring−chain equilibrium at the molecular level.[4,6,42] According to this concept, we developed a supramolecular ring−chain competition model to evaluate the intermicellar (K_{inter}) and intramicellar (K_{intra}) equilibrium constants for the supramolecular reactions of micelle subunits. Definitions of K_{inter} and K_{intra} are given as follows

$$K_{inter} = \frac{[\mathbf{M}_{i+j}]}{[\mathbf{M}_i][\mathbf{M}_j]} \quad (1)$$

$$K_{intra} = \frac{[\mathbf{C}_1]}{[\mathbf{M}_1]} \quad (2)$$

where **M** and **C** represent the micelle subunits and the cyclized product, respectively. $\mathbf{M}_1$, $\mathbf{M}_i$, and $\mathbf{M}_j$ represent the initial rodlike micelle and the formed nanowires, respectively, where the subscripts i and j are the numbers of micelle units in the nanowires (i.e., the degree of polymerization). The formed toroidal micelles are denoted as $\mathbf{C}_1$. Since the supramolecular polymerization of rodlike micelles follows the principle of step-growth manner,[26] we can obtain K_{inter} from $K_{inter} = X_n - 1$ (X_n is the number average degree of polymerization, and the details of calculation and derivation are given in Section 2.4 of the Supporting Information). By counting the number of toroidal micelles in 10 groups of simulation boxes, we estimated the concentration ratio of toroids to initial rods as the intramicellar equilibrium constant K_{intra} from eq 2.

We calculated K_{inter} and K_{intra} under various ε_{PP} at fixed ε_{RR} of 3.0ε (solid lines) and 5.0ε (dashed lines). The results are shown in Figure 5a, which corresponds to various temperatures at the fixed THF content in the experiments. Under the condition of lower ε_{PP}, K_{inter} is higher than K_{intra}, corresponding to the occurrence of polymerization. With increasing ε_{PP}, the difference between the two equilibrium constants gradually decreases. When ε_{PP} is higher than the equivalence point (the intersection in Figure 5a), K_{intra} exceeds K_{inter}, corresponding to the cyclization of rodlike micelles. The increase of ε_{RR} from 3.0ε to 5.0ε shifts the equivalence point toward the condition of higher ε_{PP}.

By employing the proposed supramolecular ring−chain equilibrium model in eqs 1 and 2, we evaluated the equilibrium constants K_{inter} and K_{intra} from the experiments. In the experiments, the mixed THF/DMF solvent (1.6 mL, THF content 60 vol %) and water (0.4 mL) were added into 1.0 mL of the rodlike micelle solution. The final THF content was 46

https://doi.org/10.1021/acs.macromol.1c01020
Macromolecules 2021, 54, 5196−5203

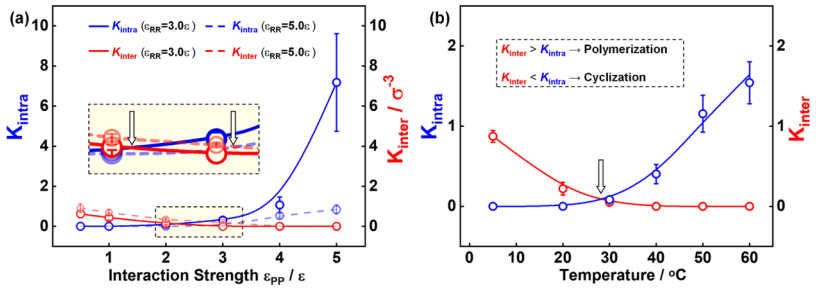

Figure 5. Variations of the intermicellar K_{inter} and intramicellar K_{intra} equilibrium constants in the supramolecular ring−chain competition, (a) The interaction parameter ε_{PP} varies from 0.5ε to 5.0ε at fixed ε_{RR} of 3.0ε (solid lines) and 5.0ε (dashed lines). (b) The temperature varies from 5 to 60 °C, and the final THF content is fixed at 46 vol %.

vol %, and the mixture solution was stabilized for 3 days at various temperatures. The number average degree of polymerization (X_n) and the fraction of toroidal morphologies were estimated from the SEM images of more than 400 micelles. For the supramolecular reactions at various temperatures, the values of K_{inter} and K_{intra} were calculated and plotted in Figure 5b. At lower temperatures, K_{inter} is higher than K_{intra}, meaning that the supramolecular polymerization is dominant. K_{inter} gradually decreases with increasing temperature. When the temperature is above 30 °C (the equivalence point in Figure 5b), K_{intra} increases, and the supramolecular cyclization occurs. In addition, the variations of K_{inter} and K_{intra} can also be regulated by varying the THF content (see Figure S13). At the lower THF content, K_{inter} is higher than K_{intra}, corresponding to the occurrence of supramolecular polymerization. With increasing THF content, K_{intra} exceeds K_{inter}, and supramolecular cyclization takes place. Therefore, the proposed ring−chain equilibrium model can well describe the supramolecular competition reaction observed in both experiments and simulations.

Supramolecular versus Molecular Ring−Chain Competition Reactions. The ring−chain competition between linear polymer chains and their cyclic counterparts is widely observed for monomers and even some oligomer units, for example, ditopic pyrimidinone, ribonuclease peptide, and oligomer units containing the bisporphyrin head and the trinitrofluorenone (TNF) tail.[9−11,16−19] In this work, we found a novel supramolecular ring−chain competition phenomenon that exhibits the following uniqueness: (1) Different kinds of interactions: Polymerization and cyclization at the molecular level are related to the covalent interaction between end groups.[3−8] In this work, the supramolecular competition involves the noncovalent hydrophobic interaction. (2) The variable conformation of reaction units: In the classical JS model for the ring−chain competition at the molecular level, the chain conformation change is ignored. Our supramolecular competition system, however, involves the bending of rodlike micelles in the cyclization. In the present work, we proposed a concept, i.e., the supramolecular ring−chain competition reaction, according to experiments, simulations, and theoretical analysis. Moreover, its ring−chain equilibrium model was proposed, which profoundly revealed the origin of such a competition reaction.

The supramolecular ring−chain competition can be used to construct various complex nanostructures by a stepwise self-assembly strategy.[20] The key is inducing out-of-equilibrium and then rebalancing the assembly system via the energy manipulation in the supramolecular ring−chain competition. For example, nanowires can be first prepared under the conditions where polymerization is dominant, and then these aggregate solutions are placed under new assembly conditions where cyclization is dominant (higher temperatures or THF-rich environment). The supramolecular ring−chain competition is moved to an out-of-equilibrium state, and then some new aggregates can be formed through the rebalancing of ring−chain competition. For example, we speculate that the nanowires can further cyclize into quaternary or polygonal ring-like structures. In addition, the curved crescent micelles formed in the cyclization process can also serve as micelle subunits to further assemble into hierarchical nanostructures via a stepwise self-assembly process. However, the expectations require the precise implementation of supramolecular reactions by the stepwise self-assembly strategy. The construction of these complex nanostructures will be the focus of our future work.

CONCLUSIONS

In summary, we report a supramolecular ring−chain competition reaction between the intermicellar polymerization and intramicellar cyclization of PBLG-*g*-PEG rodlike micelles. Nanowires, curved and toroidal micelles are obtained from such a supramolecular competition reaction, which can be regulated by the solvent composition and temperature. Lower temperatures give rise to the stronger hydrophobicity of PBLG and thereby result in the polymerization of rodlike micelles. In contrast, higher temperatures or higher THF content leads to the constriction of the pendant groups of PBLG. This constriction causes an increase in the core/shell interfacial energy and results in the intramicellar cyclization of rodlike micelles. The energy variations predicted by the simulations indicate that eliminating the unfavorable ends is the main driving force of the intermicellar polymerization, and balancing the interfacial energy and the bending energy causes the intramicellar cyclization. In the proposed supramolecular ring−chain equilibrium model, varying the intermicellar and intramicellar interactions essentially regulates the dynamic competition relation and the equilibrium constants of two supramolecular reactions. This supramolecular competition reaction provides a progressive way to construct various complex hierarchical nanostructures with controllable architectures.

ASSOCIATED CONTENT

Supporting Information

The Supporting Information is available free of charge at https://pubs.acs.org/doi/10.1021/acs.macromol.1c01020.

https://doi.org/10.1021/acs.macromol.1c01020
Macromolecules 2021, 54, 5196−5203

Details regarding experiments including the synthesis of graft copolymers and the preparation of the micelle solution; control experiments; simulation model and method; simulation results; and proposed theoretical model (PDF)

AUTHOR INFORMATION

Corresponding Authors

Liang Gao − *Shanghai Key Laboratory of Advanced Polymeric Materials, Key Laboratory for Ultrafine Materials of Ministry of Education, Frontiers Science Center for Materiobiology and Dynamic Chemistry, School of Materials Science and Engineering, East China University of Science and Technology, Shanghai 200237, China;* orcid.org/0000-0001-6852-8301; Email: lianggao@ecust.edu.cn

Jiaping Lin − *Shanghai Key Laboratory of Advanced Polymeric Materials, Key Laboratory for Ultrafine Materials of Ministry of Education, Frontiers Science Center for Materiobiology and Dynamic Chemistry, School of Materials Science and Engineering, East China University of Science and Technology, Shanghai 200237, China;* orcid.org/0000-0001-9633-4483; Email: jlin@ecust.edu.cn

Authors

Rui Hu − *Shanghai Key Laboratory of Advanced Polymeric Materials, Key Laboratory for Ultrafine Materials of Ministry of Education, Frontiers Science Center for Materiobiology and Dynamic Chemistry, School of Materials Science and Engineering, East China University of Science and Technology, Shanghai 200237, China*

Chunhua Cai − *Shanghai Key Laboratory of Advanced Polymeric Materials, Key Laboratory for Ultrafine Materials of Ministry of Education, Frontiers Science Center for Materiobiology and Dynamic Chemistry, School of Materials Science and Engineering, East China University of Science and Technology, Shanghai 200237, China;* orcid.org/0000-0001-9008-6327

Zuowei Chen − *Shanghai Key Laboratory of Advanced Polymeric Materials, Key Laboratory for Ultrafine Materials of Ministry of Education, Frontiers Science Center for Materiobiology and Dynamic Chemistry, School of Materials Science and Engineering, East China University of Science and Technology, Shanghai 200237, China*

Liquan Wang − *Shanghai Key Laboratory of Advanced Polymeric Materials, Key Laboratory for Ultrafine Materials of Ministry of Education, Frontiers Science Center for Materiobiology and Dynamic Chemistry, School of Materials Science and Engineering, East China University of Science and Technology, Shanghai 200237, China;* orcid.org/0000-0002-5141-8584

Complete contact information is available at: https://pubs.acs.org/10.1021/acs.macromol.1c01020

Notes

The authors declare no competing financial interest.

ACKNOWLEDGMENTS

This work was supported by the National Natural Science Foundation of China (51621002, 51833003, and 21975073), the China Postdoctoral Science Foundation (2020M671019), and Shanghai Sailing Program (20YF1410700).

REFERENCES

(1) De Greef, T. F.; Smulders, M. M.; Wolffs, M.; Schenning, A. P.; Sijbesma, R. P.; Meijer, E. W. Supramolecular Polymerization. *Chem. Rev.* **2009**, *109*, 5687−5754.

(2) Ercolani, G.; Mandolini, L.; Mencarelli, P.; Roelens, S. Macrocyclization under Thermodynamic Control. A Theoretical Study and Its Application to the Equilibrium Cyclooligomerization of β-Propiolactone. *J. Am. Chem. Soc.* **1993**, *115*, 3901−3908.

(3) Berkane, C.; Mezoul, G.; Lalot, T.; Brigodiot, M.; Maréchal, E. Lipase-Catalyzed Polyester Synthesis in Organic Medium. Study of Ring-Chain Equilibrium. *Macromolecules* **1997**, *30*, 7729−7734.

(4) Chen, Z.-R.; Claverie, J. P.; Grubbs, R. H.; Kornfield, J. A. Modeling Ring-Chain Equilibria in Ring-Opening Polymerization of Cycloolefins. *Macromolecules* **1995**, *28*, 2147−2154.

(5) Vermonden, T.; van der Gucht, J.; de Waard, P.; Marcelis, A. T. M.; Besseling, N. A. M.; Sudhölter, E. J. R.; Fleer, G. J.; Cohen Stuart, M. A. Water-Soluble Reversible Coordination Polymers: Chains and Rings. *Macromolecules* **2003**, *36*, 7035−7044.

(6) Yamashita, Y.; Mayumi, J.; Kawakami, Y.; Ito, K. Ring-Chain Equilibrium of Macrocyclic Formals. *Macromolecules* **1980**, *13*, 1075−1080.

(7) Hong, M.; Chen, E. Y. Completely Recyclable Biopolymers with Linear and Cyclic Topologies via Ring-Opening Polymerization of Gamma-Butyrolactone. *Nat. Chem.* **2016**, *8*, 42−49.

(8) Pang, K.; Kotek, R.; Tonelli, A. Review of Conventional and Novel Polymerization Processes for Polyesters. *Prog. Polym. Sci.* **2006**, *31*, 1009−1037.

(9) ten Cate, A. T.; Kooijman, H.; Spek, A. L.; Sijbesma, R. P.; Meijer, E. W. Conformational Control in the Cyclization of Hydrogen-Bonded Supramolecular Polymers. *J. Am. Chem. Soc.* **2004**, *126*, 3801−3808.

(10) de Greef, T. F.; Ercolani, G.; Ligthart, G. B.; Meijer, E. W.; Sijbesma, R. P. Influence of Selectivity on the Supramolecular Polymerization of AB-Type Polymers Capable of Both A•A and A•B Interactions. *J. Am. Chem. Soc.* **2008**, *130*, 13755−13764.

(11) Bastings, M. M. C.; de Greef, T. F. A.; van Dongen, J. L. J.; Merkx, M.; Meijer, E. W. Macrocyclization of Enzyme-Based Supramolecular Polymers. *Chem. Sci.* **2010**, *1*, 79−88.

(12) Paffen, T. F.; Ercolani, G.; de Greef, T. F.; Meijer, E. W. Supramolecular Buffering by Ring-Chain Competition. *J. Am. Chem. Soc.* **2015**, *137*, 1501−1509.

(13) Krug, C. K.; Nieckarz, D.; Fan, Q.; Szabelski, P.; Gottfried, J. M. The Macrocycle versus Chain Competition in On-Surface Polymerization: Insights from Reactions of 1,3-Dibromoazulene on Cu(111). *Chem. - Eur. J.* **2020**, *26*, 7647−7656.

(14) Gröger, G.; Meyer-Zaika, W.; Böttcher, C.; Gröhn, F.; Ruthard, C.; Schmuck, C. Switchable Supramolecular Polymers from the Self-Assembly of a Small Monomer with Two Orthogonal Binding Interactions. *J. Am. Chem. Soc.* **2011**, *133*, 8961−8971.

(15) Huang, Z.; Qin, B.; Chen, L.; Xu, J. F.; Faul, C. F. J.; Zhang, X. Supramolecular Polymerization from Controllable Fabrication to Living Polymerization. *Macromol. Rapid Commun.* **2017**, *38*, No. 1700312.

(16) Hirao, T.; Hisano, N.; Akine, S.; Kihara, S.-I.; Haino, T. Ring−Chain Competition in Supramolecular Polymerization Directed by Molecular Recognition of the Bisporphyrin Cleft. *Macromolecules* **2019**, *52*, 6160−6168.

(17) Reynolds, N. P.; Adamcik, J.; Berryman, J. T.; Handschin, S.; Zanjani, A. A. H.; Li, W.; Liu, K.; Zhang, A.; Mezzenga, R. Competition between Crystal and Fibril Formation in Molecular Mutations of Amyloidogenic Peptides. *Nat. Commun.* **2017**, *8*, No. 1338.

(18) Xiao, T.; Feng, X.; Ye, S.; Guan, Y.; Li, S.-L.; Wang, Q.; Ji, Y.; Zhu, D.; Hu, X.; Lin, C.; Pan, Y.; Wang, L. Highly Controllable Ring−Chain Equilibrium in Quadruply Hydrogen Bonded Supramolecular Polymers. *Macromolecules* **2012**, *45*, 9585−9594.

(19) Xu, J.; Huang, Z.; Chen, L.; Qin, B.; Song, Q.; Wang, Z.; Zhang, X. Supramolecular Polymerization Controlled by Reversible Conformational Modulation. *ACS Macro Lett.* **2015**, *4*, 1410−1414.

(20) Lu, Y.; Lin, J.; Wang, L.; Zhang, L.; Cai, C. Self-Assembly of Copolymer Micelles: Higher-Level Assembly for Constructing Hierarchical Structure. *Chem. Rev.* **2020**, *120*, 4111−4140.
(21) Shen, B.; Zhu, Y.; Kim, Y.; Zhou, X.; Sun, H.; Lu, Z.; Lee, M. Autonomous Helical Propagation of Active Toroids with Mechanical Action. *Nat. Commun.* **2019**, *10*, No. 1080.
(22) Gröschel, A. H.; Schacher, F. H.; Schmalz, H.; Borisov, O. V.; Zhulina, E. B.; Walther, A.; Müller, A. H. Precise Hierarchical Self-Assembly of Multicompartment Micelles. *Nat. Commun.* **2012**, *3*, No. 710.
(23) Gröschel, A. H.; Walther, A.; Lobling, T. I.; Schacher, F. H.; Schmalz, H.; Müller, A. H. Guided Hierarchical Co-Assembly of Soft Patchy Nanoparticles. *Nature* **2013**, *503*, 247−251.
(24) Li, X.; Gao, Y.; Boott, C. E.; Winnik, M. A.; Manners, I. Non-Covalent Synthesis of Supermicelles with Complex Architectures Using Spatially Confined Hydrogen-Bonding Interactions. *Nat. Commun.* **2015**, *6*, No. 8127.
(25) Gu, M.; Ma, X.; Zhang, L.; Lin, J. Reversible Polymerization-like Kinetics for Programmable Self-Assembly of DNA-Encoded Nanoparticles with Limited Valence. *J. Am. Chem. Soc.* **2019**, *141*, 16408−16415.
(26) Zhuang, Z.; Jiang, T.; Lin, J.; Gao, L.; Yang, C.; Wang, L.; Cai, C. Hierarchical Nanowires Synthesized by Supramolecular Stepwise Polymerization. *Angew. Chem., Int. Ed.* **2016**, *55*, 12522−12527.
(27) Tu, Y.; Ji, Z.; Yang, X.; Wan, X.; Zhou, Q. Supramolecular Chemistry in the Formation of Self-Assembled Nanostructures from a High-Molecular-Weight Rod-Coil Block Copolymer. *Macromol. Rapid Commun.* **2014**, *35*, 1795−1800.
(28) Gao, H.; Ma, X.; Lin, J.; Wang, L.; Cai, C.; Zhang, L.; Tian, X. Synthesis of Nanowires via Temperature-Induced Supramolecular Step-Growth Polymerization. *Macromolecules* **2019**, *52*, 7731−7739.
(29) Yang, C.; Gao, L.; Lin, J.; Wang, L.; Cai, C.; Wei, Y.; Li, Z. Toroid Formation through a Supramolecular "Cyclization Reaction" of Rodlike Micelles. *Angew. Chem., Int. Ed.* **2017**, *56*, 5546−5550.
(30) Gao, L.; Hu, R.; Xu, P.; Lin, J.; Zhang, L.; Wang, L. Supramolecular Cyclization of Semiflexible Cylindrical Micelles Assembled from Rod-Coil Graft Copolymers. *Nanoscale* **2020**, *12*, 296−305.
(31) Adler, A. J.; Hoving, R.; Potter, J.; Wells, M.; Fasman, G. D. Circular Dichroism of Polypeptides. Poly(hydroxyethyl-L-glutamine) compared to Poly(L-glutamic acid). *J. Am. Chem. Soc.* **1968**, *90*, 4736−4738.
(32) Łosik, M.; Kubowicz, S.; Smarsly, B.; Schlaad, H. Solid-State Structure of Polypeptide-Based Rod-Coil Block Copolymers: Folding of Helices. *Eur. Phys. J. E* **2004**, *15*, 407−411.
(33) Guo, A.; Yang, W.; Yang, F.; Yu, R.; Wu, Y. Well-Defined Poly(γ-benzyl-$_L$-glutamate)-*g*-Polytetrahydrofuran: Synthesis, Characterization, and Properties. *Macromolecules* **2014**, *47*, 5450−5461.
(34) Heitz, F.; Marchal, E.; Spach, G. Side-Chain Interactions and Conformation in α-Helical Poly(γ-phenacyl L-glutamate). Aggregation in Dilute Solutions. *Macromolecules* **1975**, *8*, 145−151.
(35) Magnotti, E. L.; Hughes, S. A.; Dillard, R. S.; Wang, S.; Hough, L.; Karumbamkandathil, A.; Lian, T.; Wall, J. S.; Zuo, X.; Wright, E. R.; Conticello, V. P. Self-Assembly of an α-Helical Peptide into a Crystalline Two-Dimensional Nanoporous Framework. *J. Am. Chem. Soc.* **2016**, *138*, 16274−16282.
(36) Le Fer, G.; Wirotius, A. L.; Brûlet, A.; Garanger, E.; Lecommandoux, S. Self-Assembly of Stimuli-Responsive Biohybrid Synthetic-*b*-Recombinant Block Copolypeptides. *Biomacromolecules* **2019**, *20*, 254−272.
(37) Horsch, M. A.; Zhang, Z.; Glotzer, S. C. Self-Assembly of Polymer-Tethered Nanorods. *Phys. Rev. Lett.* **2005**, *95*, No. 056105.
(38) Grest, G. S.; Kremer, K. Molecular Dynamics Simulation for Polymers in the Presence of A Heat Bath. *Phys. Rev. A* **1986**, *33*, 3628−3631.
(39) Marson, R. L.; Phillips, C. L.; Anderson, J. A.; Glotzer, S. C. Phase Behavior and Complex Crystal Structures of Self-Assembled Tethered Nanoparticle Telechelics. *Nano Lett.* **2014**, *14*, 2071−2078.
(40) Asgari, M. A Molecular Model for the Free Energy, Bending Elasticity, and Persistence Length of Wormlike Micelles. *Eur. Phys. J. E* **2015**, *38*, No. 98.
(41) Hoang, T. X.; Giacometti, A.; Podgornik, R.; Nguyen, N. T.; Banavar, J. R.; Maritan, A. From Toroidal to Rod-like Condensates of Semiflexible Polymers. *J. Chem. Phys.* **2014**, *140*, No. 064902.
(42) Jacobson, H.; Stockmayer, W. H. Intramolecular Reaction in Polycondensations. I. The Theory of Linear Systems. *J. Chem. Phys.* **1950**, *18*, 1600−1606.

https://doi.org/10.1021/acs.macromol.1c01020
Macromolecules 2021, 54, 5196−5203